



Comprehensive Design Procedure and Manufacturing of Permanent Magnet Assisted Synchronous Reluctance Motor

H. Aghazadeh^a, E. Afjei^{*a}, A. Siadatan^b

^a Department of Power Electrical Engineering, Faculty of Electrical Engineering, University of Shahid Beheshti, Tehran, Iran

^b Department of Energy Systems, Faculty of Applied Science & Engineering, University of Toronto, Toronto, Ontario, Canada

PAPER INFO

Paper history:

Received 07 May 2019

Received in revised form 25 May 2019

Accepted 05 July 2019

Keywords:

Finite Element Method

Magnetic Flux Barrier

Motor

Synchronous Reluctance

Torque Ripple

ABSTRACT

Combining the main advantages of the permanent magnet synchronous motors and pure synchronous reluctance motors (SynRM), permanent magnet assisted synchronous reluctance motor (PMA SynRM) has been considered as a promising alternative to the conventional induction motors. In this paper, utilizing a macroscopic design parameter, called insulation ratio along the q-axis, and based on the magnetic reluctance concept, a simple and fast design procedure of synchronous reluctance motor is introduced. Then, the performance improvement of the machine by inserting the permanent magnets into the rotor body is investigated. After calculating the width of the magnetic flux barriers two dimensions Finite Element Method (FEM) analysis simulation of the designed motor is presented. Additionally, the performance characteristics of the designed motor such as torque producing capability and torque ripple are discussed. Furthermore, thermal analysis is conducted to determine the temperature distribution in the designed motor. Consequently, the prototype motor is fabricated and the experimental results are compared to the simulation results which validate the usefulness of the design method.

doi: 10.5829/ije.2019.32.09c.10

1. INTRODUCTION

Nowadays, there is an increasing tendency to use energy efficient electrical machines among which reluctance machines, both switched reluctance machines (SRM) and synchronous reluctance machines (SynRM), are of great interest [1–3]. High efficient, low cost, robust rotor structure, no rotor winding, hence no copper losses features of SynRM make it one of the most promising alternatives for costly permanent magnet machines (PM) or low efficient induction machines (IM) [4, 5]. However, if SynRM does not have large enough magnetizing inductance difference along the two orthogonal axes, called d- and q axes, and suitable saliency ratio on the rotor structure as well, it will suffer from its poor performance characteristics such as low average torque, high torque ripple, and low power factor [6]. Therefore, a vast amount of efforts has been dedicated to the rotor design of SynRM where the idea of using multi-layer flux barriers has used widely [7].

However, for a same level of output power SynRM without magnet would have higher volume compared to the conventional induction motors or PM motors [7–9]. Therefore, the suggestion of placing magnets into the rotor cavities can provide further improvement in the torque producing capability of permanent magnet assisted SynRM (PMA SynRM). On the other hand, the torque pulsation is a crucial term in the quality of the produced torque [9, 10]. Cogging torque effect, as a result of utilizing magnets, on the output torque should be considered in the PMA SynRM design stage [11]. Most of the studies on SynRM design have focused on the flux barrier shape optimization with different objective functions such as maximizing the average torque and minimizing torque ripple. While the rotor has a complex structure innately, the flux barrier involves too many geometric parameters to optimize. Generally, two possible solutions have suggested in literature: (a) running parametric sensitivity analysis through implementation of the different cases by finite element

*Corresponding Author Email: e-afjei@sbu.ac.ir (E. Afjei)

method (FEM) [12, 13] (b) utilizing lumped parameter model (LPM) of the cases and solving the magnetic circuit analytically [11, 14]. Whereas the former method is time consuming but the results are almost precise, the latter is fast but the inaccuracy of the provided results should be corrected by conducting some FEM simulations [15].

To deal with this challenge in the rotor design, this paper presents a combined analytic – FEM based method which uses a macroscopic parameter, called insulation ratio, to link the microscopic geometric parameters.

2. PRINCIPLE OF SYNCHRONOUS RELUCTANCE MOTOR

SynRM works based on a variable reluctance concept where there are two different paths for the flux lines produced by the stator winding on the air-gap. The path through the iron segment of the rotor is called direct axis (*d*-axis) which has minimum magnetic resistance (minimum reluctance), as shown in Figure 1. The other path with maximum reluctance, which contains magnetic flux barriers, is called quadratic axis (*q*-axis). Figure 1 shows a typical 4 pole PMSynRM with three flux barriers in each pole.

The output torque equation of the SynRM after inserting the magnets into the flux barriers is defined as follows [16]:

$$T_{em} = \frac{3}{2} p (\lambda_{pm} i_{dm} + (L_{dm} - L_{qm}) i_{qm} i_{dm}) \tag{1}$$

where *p* is pole pair number of the motor, λ_{pm} is the permanent magnet flux linkage, i_{dm} , i_{qm} are stator current components and L_{dm} , L_{qm} are magnetizing inductances in *d*- and *q*-axes, respectively. Equation (1) illustrates the produced torque of PMSynRM has two parts: first, the reluctance torque as a result of salient rotor structure, and second the permanent magnet resultant torque.

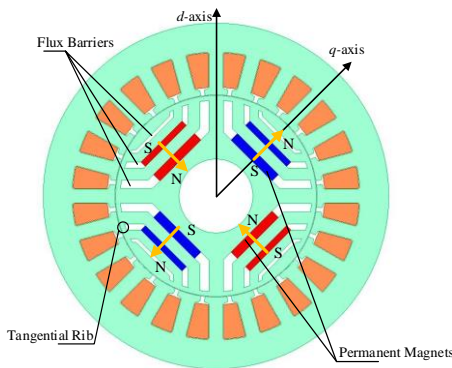


Figure 1. Sketch of 4 pole PMSynRM

3. ROTOR DESIGN OF SYNRM

Flux barriers inside the rotor body may have different shapes depending on the general specifications of the SynRM such pole number of the motor, stator slot shape and so on. In order to define the rotor geometric parameters and simultaneously to facilitate the parametric sensitivity analysis on the initial design, a rotor shown in Figure 2 with rationally shaped flux barriers is selected. The shapes and positions of the flux barriers are defined by calculation the widths of flux barriers (W_{bi}) and flux carriers (S_i) along the *q*-axis and also by determining the end point angles of the flux barriers on the periphery of the rotor. Additionally, a virtual point with angle β with respect to *q*-axis is used to adjust the end point angles.

At the first step, the magneto motive force (MMF) produced by the stator winding simplistically is assumed to have a sinusoidal distribution over the air-gap. Considering uniform distribution of the end points of the flux barriers ($\alpha_m = \text{constant}$), staircase distributions of the stator MMF in the *d*- and *q*-axes on the rotor for $\beta = 0$ are shown in Figure 3. Figure 3 shows adjusting the angle β changes the end point angle of each flux barrier (α_i). Therefore, for a certain value of the motor pole number (*P*), number of barriers (n_b) and for a known β , the end

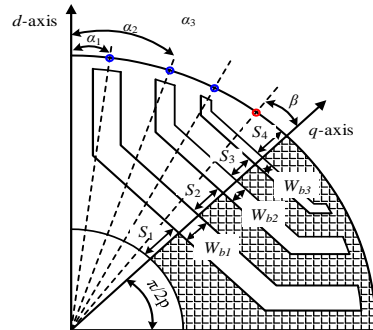


Figure 2. One pole view of the rotor including rotor design parameters

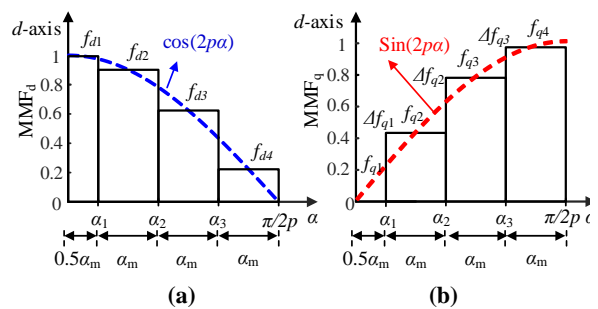


Figure 3. Magneto motive force distribution (p.u): (a) MMF_d for $\beta = 0$, (b) MMF_q for $\beta = 0$

points pitch angle is defined [18]:

$$\alpha_m = \frac{((\pi / P) - 2\beta)}{(2n_b + 1)} \quad (2)$$

Two general rules are applied to calculate the widths of flux barriers and flux carriers. Firstly, considering “homogeneous salient rotor” concept, the permeance ratio of the flux barriers (p_i/p_j) is constant and then the widths of two adjacent flux barriers are proportional to the average MMF_q difference as follows [16]:

$$\frac{p_i}{p_j} = cte. \Rightarrow \frac{W_{bi}}{W_{bj}} = \left(\frac{\Delta f_i}{\Delta f_j}\right)^2 \quad i = 2, \dots, n_b \quad (3)$$

$$\Delta f_i = f_{qi+1} - f_{qi} \quad i = 1, \dots, n_b - 1$$

Figures 3(b) and 3(d) show the sinusoidal distribution of MMF_q over the half pole view of the rotor.

Secondly, as Figures 3 (a) and 3(c) show, the iron segments widths are directly proportional to the flowing flux. Then, the width of flux carriers are calculated by Moghaddam and Gyllensten [17]:

$$\begin{cases} \frac{2S_1}{S_2} = \frac{f_{d1}}{f_{d2}} \\ \frac{S_{i+1}}{S_i} = \frac{f_{di+1}}{f_{di}} \quad i = 2, \dots, n_b \end{cases} \quad (4)$$

It is worth noting, as the d -axis is in the middle of the first iron segment, to calculate the width of the first carrier it is assumed that $2S_1$ is proportional to f_{d1} . Applying this rule makes the uniform utilization of the iron segments possible.

With the aim of connecting the microscopic parameters involved in the rotor geometry, the insulation ratio is defined as Equation (5) where l_a is total insulation along the q -axis, l_y is total iron portion, D_{si} is inner diameter of the stator, D_{sh} is shaft diameter, and g is the air gap length.

$$k_{wq} = \frac{l_a}{l_y} = \frac{\frac{D_{si}}{2} - g - \frac{D_{sh}}{2} - \sum_{k=1}^{nb+1} S_k}{\sum_{k=1}^{nb+1} S_k} \quad (5)$$

Using equation Equation (5), total insulation along the q -axis is defined as follows:

$$l_a = \sum_{i=1}^{nb} W_{bi} = \frac{\frac{D_{si}}{2} - g - \frac{D_{sh}}{2}}{1 + \frac{1}{k_{wq}}} \quad (6)$$

Rearranging the presented equations and solving a linear equation system, n_b unknown widths of the flux barriers can be calculated:

$$\mathbf{GW} = \mathbf{H} \quad (7)$$

$$\mathbf{G} = \begin{pmatrix} 1 & 1 & 1 & \dots & 1 \\ 1 & -\left(\frac{\Delta f_1}{\Delta f_2}\right)^2 & 0 & \dots & 0 \\ 0 & 1 & -\left(\frac{\Delta f_2}{\Delta f_3}\right)^2 & \ddots & \vdots \\ \vdots & \ddots & \ddots & \ddots & 0 \\ 0 & \dots & 0 & 1 & -\left(\frac{\Delta f_{n_b-1}}{\Delta f_{n_b}}\right)^2 \end{pmatrix}_{(n_b \times n_b)}$$

$$\mathbf{W} = (W_{b1} \quad \dots \quad W_{bn_b})_{(n_b \times 1)}^T$$

$$\mathbf{H} = (l_a \quad 0 \quad \dots \quad 0)_{(n_b \times 1)}^T$$

Moreover, the n_b+1 unknown widths of the flux carriers can be determined as follows:

$$\mathbf{FS} = \mathbf{D} \quad (8)$$

$$\mathbf{S} = (S_1 \quad \dots \quad S_{nb+1})_{(nb+1 \times 1)}^T$$

$$\mathbf{D} = (l_a + l_y \quad 0 \quad \dots \quad 0)_{(nb+1 \times 1)}^T$$

$$\mathbf{F} = \begin{pmatrix} 1+k_{wq} & 1+k_{wq} & 1+k_{wq} & \dots & 1+k_{wq} \\ 2f_{d2} & -f_{d1} & 0 & \dots & 0 \\ 0 & f_{d3} & -f_{d2} & \ddots & \vdots \\ \vdots & \ddots & \ddots & \ddots & 0 \\ 0 & \dots & 0 & f_{dn_b+1} & -f_{dn_b} \end{pmatrix}_{(nb+1 \times nb+1)}$$

It is worthwhile to mention that the optimum value of insulation ratio is selected based on running a limited number of parametric sensitivity analysis.

4. FINITE ELEMENT ANALYSIS RESULTS

The rotor design procedure described in the previous section is applied to a motor with general specifications provided in Table 1. The resultant 2D model of the motor is implemented and then sensitivity analysis results of the initial design are presented in Figure 4. The provided simulation results in this section are for 2.2 A stator current and rated speed of 1500 rpm. According to the Figure 4 the output torque has a maximum of 4.25 N.m at 0.6 value of insulation ratio. Therefore, the optimum value of the insulation ratio is determined by running only six simulation cases.

TABLE 1. General specification of the motor

Symbol	Definition	Value
P_n	Rated power	745 W
N_s	Rated speed	1500 rpm
P	No. of poles	4
Q_s	No. of stator slots	24
n_b	No. of flux barriers	3
G	Air-gap length	0.35 mm
D_{si}	Inner Diameter of stator	70 mm
D_{sh}	Shaft diameter	25 mm

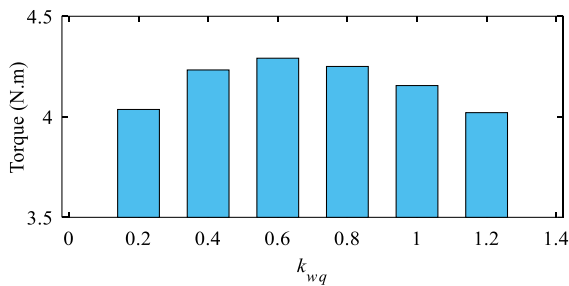


Figure 4. Sensitivity analysis result, output average torque in terms of insulation ratio

Furthermore, in order to consider the effect of angle β on the output torque ripple, Figure 5 shows the torque profile for two values of β . It is clear by changing the β from 0 to $0.5\alpha_m$ the torque ripple is decreased from 60% to 44.6%. Therefore, β can be used to adjust the output torque ripple of SynRM.

Although utilizing β increases the number of degrees of freedom, the end points pitch angle α_m is constant. In order to expand the search area, the end points of the barriers can be distributed non-uniformly. Subsequently, the output torques with maximum average and minimum torque ripple are shown in Figure 6. Summing up, non-uniform distribution of the end points reduces the torque ripple from 32.88% to 18.2% though the average torque is decreased as well.

However, one of the common issues associated to the PMSynRM is cogging torque. Cogging torque makes

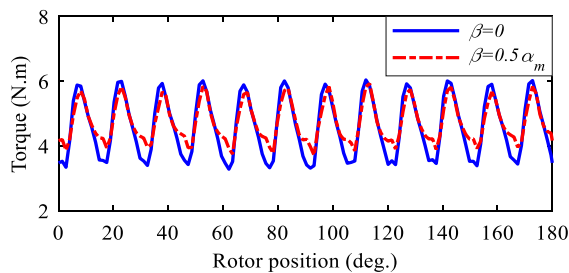


Figure 5. Output torque of SynRM for two values of β

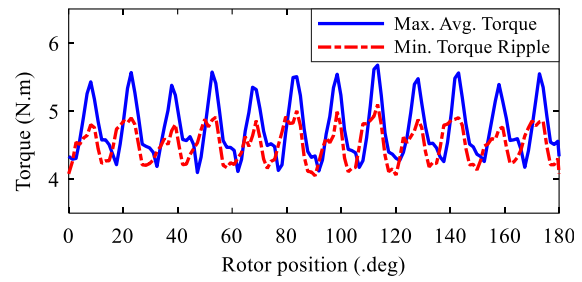


Figure 6. Output torque of SynRM with maximum average torque and minimum torque ripple

the motor noisy and decreases the bearings life drastically. Cogging torque of PMSynRM with two widths of magnets is shown in Figure 7. Although, increasing the width of magnets increases the maximum cogging torque from 22 mN.m to 54 mN.m, it also elevates the output torque, which is shown in Figure 8. To ensure a safe operation of the designed motor, thermal distribution of SynRM is presented in Figure 9. As the copper losses of the stator winding are the main source of heating, the hot spot area is around the stator slots.

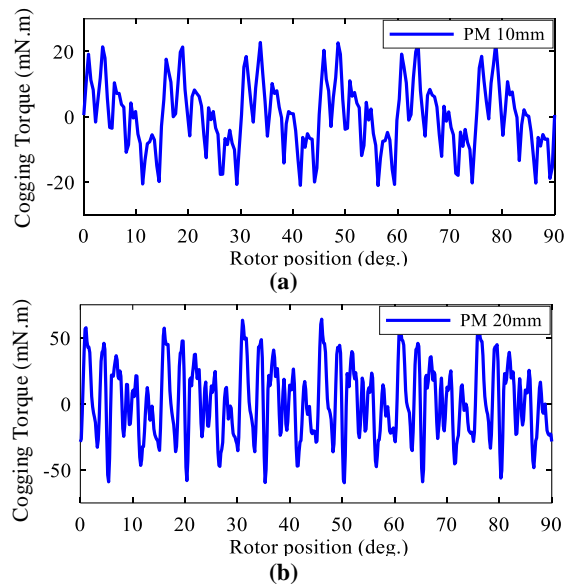


Figure 7. Cogging torque: (a) SynRM, and (b) PMSynRM

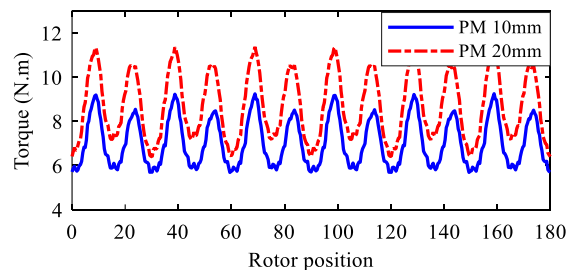


Figure 8. Output torque of PMSynRM with two magnet sizes

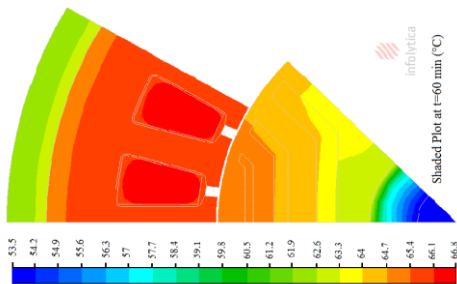


Figure 9. Thermal distribution of SynRM

5. MEASUREMENT RESULTS

Prototype of the designed SynRM is shown in Figure 10. In order to validate the simulation results, the prototyped motor is tested by the provided test-bench in Figure 11. Firstly, based on the locked rotor test the phase inductance of the motor is compared by the FEM simulation results in Figure 12. Although there is a slight difference, the measured inductance trend is as same as the FEM result. Secondly, the output torques of the cases, SynRM and PMSynRM, at the rated speed of 1500 rpm and 2.2 stator current (shown in Figure 13) are compared with simulation results in Figure 14.

According to the presented results, generally measurement results are lower than simulation results though the fabricated PMSynRM has higher performance characteristics in terms of average torque, torque ripple and power factor. The reason for the difference between FEM and experimental results are the mechanical implementation inaccuracy in addition to the materials used to prototype the motor. However, the comparison of experimental results of the SynRM and PMSynRM are in a good agreement with the simulation results by the FEM analysis.

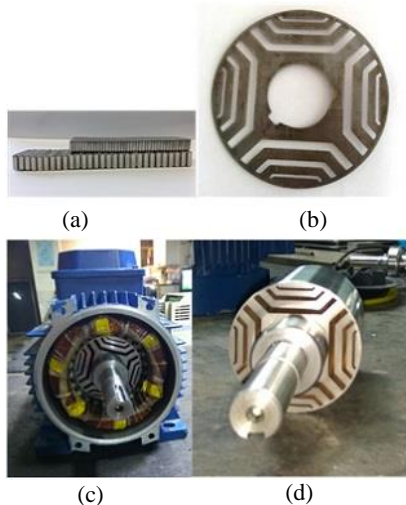


Figure 10. Prototype of the SynRM: (a) NdFeB magnets, (b) rotor lamination, (c) stator and rotor of SynRM, and (d) rotor

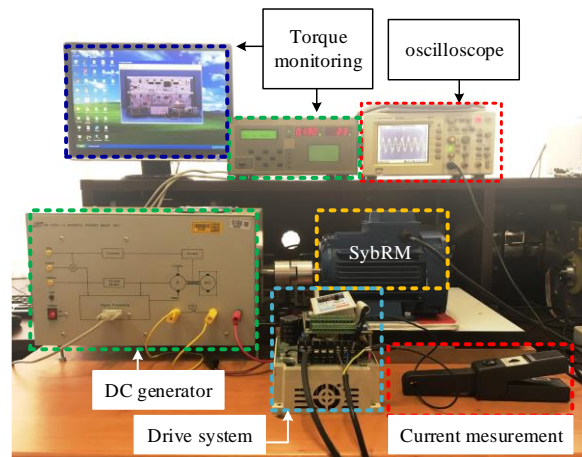


Figure 11. Test-bench of the prototyped SynRM

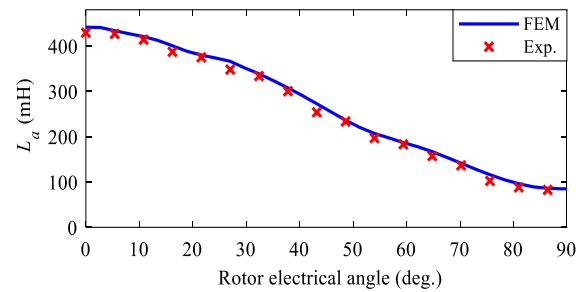


Figure 12. Phase inductance of the prototyped SynRM

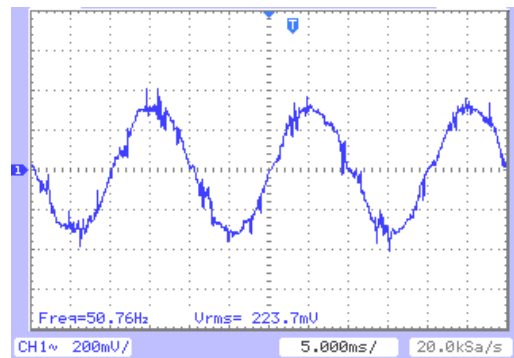
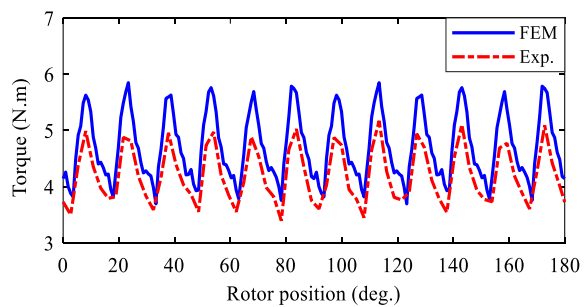
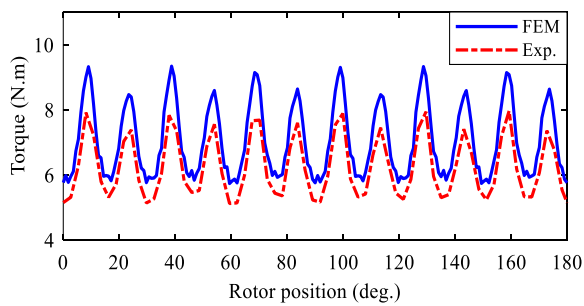


Figure 13. Phase current of the prototyped SynRM



(a)



(b)

Figure 14. FEM and experimental Output torque comparison: (a) SynRM, and (b) PMaSynRM

6. CONCLUSION

In this paper, a simple and fast rotor design procedure of SynRM is proposed. The insulation ratio is an effective parameter to link the geometric parameters involved in the rotor structure where the main design goal is to maximize the output torque. Moreover, the effect of the end point angles of the flux barriers on the torque ripple is considered. Furthermore, the pros and cons of placing the permanent magnets into the flux barriers in PMaSynRM are discussed. Based in the FEM and experimental measurement results PMaSynRM has higher torque producing capability in comparison to the pure SynRM.

7. REFERENCES

- Soltani, J. and Zarchi, H. A., "Robust optimal speed tracking control of a current sensorless synchronous reluctance motor drive using a new sliding mode controller," *International Journal of Engineering -Transaction B: Applications*, Vol. 17, No. 2, (2004), 155–170.
- Rafiee, M., Afjeib, E. and Siadatana, A., "Design, Construction and Comparison of a Sensorless Driver Circuit for Switched Reluctance Motor," *International Journal of Engineering - Transaction A: Basics*, Vol. 27, No. 1, (2014), 143–156.
- Shafagh, E. and Faiz, J., "Influence of Operation Conditions Upon the Dynamic Steady State Performance of Switched Reluctance Motor," *International Journal of Engineering - Transaction A: Basics*, Vol. 12, No. 4, (1999), 219–232.
- Bolognani, S., Mahmoud, H., and Bianchi, N., "Fast synthesis of permanent magnet assisted synchronous reluctance motors," *IET Electric Power Applications*, Vol. 10, No. 5, (2016), 312–318.
- Torkaman, H., Ghaheri, A., and Keyhani, A., "Design of Rotor Excited Axial Flux-Switching Permanent Magnet Machine," *IEEE Transactions on Energy Conversion*, Vol. 33, No. 3, (2018), 1175–1183.
- Kostko, J.K., "Polyphase reaction synchronous motors," *Journal of the American Institute of Electrical Engineers*, Vol. 42, No. 11, (1923), 1162–1168.
- Okamoto, Y., Hoshino, R., Wakao, S. and Tsuburaya, T., "Improvement of Torque Characteristics For a Synchronous Reluctance Motor Using MMA-based Topology Optimization Method," *IEEE Transactions on Magnetics*, Vol. 54, No. 3, (2018), 1–4.
- Huang, P.W., Tsai, M.C., and Jiang, I.H., "3-D Structure Line-Start Synchronous Reluctance Motor Design Based on Selective Laser Melting of 3-D Printing," *IEEE Transactions on Magnetics*, Vol. 54, No. 11, (2018), 1–4.
- Payza, O., Demir, Y., and Aydin, M., "Investigation of Losses for a Concentrated Winding High-Speed Permanent Magnet-Assisted Synchronous Reluctance Motor for Washing Machine Application," *IEEE Transactions on Magnetics*, Vol. 54, No. 11, (2018), 1–5.
- Bonthu, S.S.R., Tarek, M.T.B., and Choi, S., "Optimal Torque Ripple Reduction Technique for Outer Rotor Permanent Magnet Synchronous Reluctance Motors," *IEEE Transactions on Energy Conversion*, Vol. 33, No. 3, (2018), 1184–1192.
- Bonthu, S.S.R., Choi, S., and Baek, J., "Design Optimization With Multiphysics Analysis on External Rotor Permanent Magnet-Assisted Synchronous Reluctance Motors," *IEEE Transactions on Energy Conversion*, Vol. 33, No. 1, (2018), 290–298.
- Raj, M.A. and Kavitha, A., "Effect of Rotor Geometry on Peak and Average Torque of External-Rotor Synchronous Reluctance Motor in Comparison With Switched Reluctance Motor for Low-Speed Direct-Drive Domestic Application," *IEEE Transactions on Magnetics*, Vol. 53, No. 11, (2017), 1–8.
- Taghavi, S.M. and Pillay, P., "A Mechanically Robust Rotor With Transverse Laminations for a Wide-Speed-Range Synchronous Reluctance Traction Motor," *IEEE Transactions on Industry Applications*, Vol. 51, No. 6, (2015), 4404–4414.
- Watanabe, K., Suga, T., and Kitabatake, S., "Topology Optimization Based on the ON/OFF Method for Synchronous Motor," *IEEE Transactions on Magnetics*, Vol. 54, No. 3, (2018), 1–4.
- Lovelace, E.C., Jahns, T.M., and Lang, J.H., "A saturating lumped-parameter model for an interior PM synchronous machine," *IEEE Transactions on Industry Applications*, Vol. 38, No. 3, (2002), 645–650.
- Moghaddam, R.R. and Gyllensten, F., "Novel High-Performance SynRM Design Method: An Easy Approach for A Complicated Rotor Topology," *IEEE Transactions on Industrial Electronics*, Vol. 61, No. 9, (2014), 5058–5065.
- Bonthu, S.S.R., Choi, S. and Baek, J., "Comparisons of three-phase and five-phase permanent magnet assisted synchronous reluctance motors," *IET Electric Power Applications*, Vol. 10, No. 5, (2016), 347–355.

Comprehensive Design Procedure and Manufacturing of Permanent Magnet Assisted Synchronous Reluctance Motor

H. Aghazadeh^a, E. Afjei^a, A. Siadatan^b

^a Department of Power Electrical Engineering, Faculty of Electrical Engineering, University of Shahid Beheshti, Tehran, Iran

^b Department of Energy Systems, Faculty of Applied Science & Engineering, University of Toronto, Toronto, Ontario, Canada

P A P E R I N F O

چکیده

Paper history:

Received 07 May 2019

Received in revised form 25 May 2019

Accepted 05 July 2019

Keywords:

Finite Element Method

Magnetic Flux Barrier

Motor

Synchronous Reluctance

Torque Ripple

موتور رلوکتانس سنکرون با آهنربای دائم کمکی به دلیل داشتن مزایای دو موتور سنکرون آهنربای دائمی و موتور رلوکتانس سنکرون یکی از نامزدهای اصلی برای جایگزینی موتورهای القایی در نظر گرفته شده است. در این مقاله، با معرفی یک پارامتر طراحی درشت‌نمود با نام نسبت عایقی در راستای محور q ، روش طراحی موتور رلوکتانس سنکرون ارائه شده و استفاده از آهنربای دائم برای بهبود مشخصه‌های عملکرد موتور از جمله چگالی گشتاور و ضریب توان موتور بررسی شده است. در این روش با استفاده از مفاهیم بنیادی طراحی ماشین و اصل مقاومت مغناطیسی متغییر، ابعاد لایه‌های سد مغناطیسی و موقعیت نقاط انتهایی لایه‌های سد در داخل روتور محاسبه شده و موتور طراحی شده در نرم افزار اجزاء محدود بصورت دو بعدی شبیه سازی شده است. همچنین با انجام تحلیل حرارتی نحوه توزیع حرارت در قسمت‌های مختلف موتور مشخص شده است. در پایان نمونه آزمایشگاهی موتور طراحی شده ساخته شده و مورد آزمایش قرار گرفته است. نتایج اندازه‌گیری عملی صحت نتایج حاصل از شبیه سازی را تایید می‌کنند.

doi: 10.5829/ije.2019.32.09c.10